SHAPE PRIOR BASED SEGMENTATION FOR ORGAN DEFORMATION CORRECTION

Jun Xie and Hung-tat Tsui*

Electronic Engineering Department
The Chinese University of Hong Kong
Shatin, N.T., Hong Kong

Wai Man Lam, Wynnie

Faculty of Medicine
The Chinese University of Hong Kong
Shatin, N.T., Hong Kong

ABSTRACT

This paper presents a real-time framework to achieve accurate deformation compensation using intra-operative Ultrasound (US) with pre-operative Magnetic Resonance Imaging (MRI). It includes a shape prior based segmentation process and a warping computation. Given two different module templates of a region of interest (ROI), the method can extract the same ROI from new real-time images based on the shape prior model in the level set space. Then the segmentation result and the matching transformation are used to simulate deformation on MR images. Through experimental results, we show that this novel segmentation method can find the shape of ROI accurately. It can provide a good assistance for real-time simulation of organ deformation.

1. INTRODUCTION

In Computer Assisted Surgery, it is essential to complement human visual systems with computer vision. Today, most image-guided surgeries rely on the high degree of correspondence between the pre-operative images and the patient anatomy under operation. The errors of the correspondence are caused mainly by the geometrical distortions and tissue deformation. The most popular method to solve the deformation problem is to correlate intra-operative US with pre-operative MRI because of its low cost, simplicity, and comparatively mature 2D/3D image registration technologies.

Cootes et al. [1] proposed the Active Shape Models (ASM) which relies on the statistics of an object's shape and gray-level appearances gathered from a training set of manual land-marks of the object. Arbel et al. [2] matched pre-operative MR images to intra-operative US images hierarchically and recursively, based on cross-correlation similarity. Pennec et al. [3] handled this problem by two steps: first conducted rigid pre-operative MR/US image registration, then ran a non-rigid tracking between pre- and intra-operative US image sequences. They finally applied the deformation field of tracking to compensate the MR images. Aylward *et al.* [4] introduced an interesting automated and accurate registration method based on the visible vessels in images.

In this paper, given two registered pre-operative images including an US image and a correspondingly reformed MR image, we proposed a framework to simulate the deformation on the MR image space according to an intra-operative US image. As the method in [3], our method also applies pre-operative US images because the shape prior from an US template has great advantages for the real-time segmentation process. Our approach includes two steps. First, the real-time shape of the ROI is extracted from the intra-operative US image through a simple shape prior based segmentation method. Second, based on the obtained real-time shape and the transformation between the pre-operative and intra-operative shapes, the warping of the MRI template is computed by correspondence matching and interpolated transformation.

2. SHAPE PRIOR BASED SEGMENTATION

Several authors have proposed their methods to incorporate the shape prior into the Geometric Active Contours. One of the most used methods to model the prior shapes is statistic modelling. Rousson et al. [5] present a method to recover a segmentation map based on global-to-local registration and prior region statistic properties. In [6], segmentation is implemented by two steps: initial segmentation and its correction based on a shape prior model. The model is obtained through a PCA which is also used in [7]. In [8], shapes are represented using a collection of points. It applies clustering methods instead of statistical methods to get the shape prior model. The similarity of shapes is measured by area information which is very high time-consuming.

In our method, we use an edge matching approach to incorporate the shape prior into the segmentation scheme. In 2D space, let $\Psi_S : \Omega \rightarrow \Re^+$ be a Lipchitz function that refers to a level set representation for a given shape S. This shape defines a region $\Re$ in the image plane Ω. Given these

*The work was partially supported by Project no. CUHK1/00C from the Research Grants Council of the Hong Kong Special Administrative Region.

0-7803-8554-3/04/$20.00 ©2004 IEEE.

definitions the following shape representation is considered

$$\Psi_S(x,y) = \begin{cases} 0, & (x,y) \in S \\ D((x,y),S), & (x,y) \in \Re_S \\ -D((x,y),S), & (x,y) \in [\Omega - \Re_S] \end{cases} \quad (1)$$

where $D((x,y),S)$ refers to the min Euclidean distance between the grid location (x,y) and the shape S. Two edges are aligned by minimizing the difference Q defined as

$$Q = \sum_{i=1}^{n} f^2(p_i). \quad (2)$$

where n the number of points on the contour and $f(p_i)$ the matching gradient of p_i defined as

$$f(p_i) = \Psi_S(T'(x_i, y_i)) \quad (3)$$

T is a similarity transformation as

$$\begin{bmatrix} X \\ Y \end{bmatrix} = T \begin{bmatrix} x \\ y \end{bmatrix} = s \begin{bmatrix} \cos(\phi) & \sin(\phi) \\ -\sin(\phi) & \cos(\phi) \end{bmatrix} \begin{bmatrix} x \\ y \end{bmatrix} + \begin{bmatrix} T_x \\ T_y \end{bmatrix} \quad (4)$$

where s is the scale parameter, ϕ is the rotation angle and (T_x, T_y) are the translation parameters in the X and Y directions.

At the beginning of the segmentation, the shape prior is posted on the test image and the matching gradient map is constructed by calculating the matching gradient of each point in the image. Then in each following iteration of propagation, the curve is updated by minimizing the following energy function

$$E(\Phi) = \int_{\Omega} (\alpha G + (1-\alpha)Q)|\nabla\Phi| dp \quad (5)$$

where G is an edge penalty function and α is a blending parameter between the two energy terms. The matching gradient value of each point on the new contour is approximated by the value of the corresponding point on the matching gradient map. The map is updated after several evolving iterations by a new matching process by minimizing Eq. (2). These two steps alternate until the system reaches a steady-state solution.

In order to minimize a least squares function such as Eq. (2), we define a matrix $\mathbf{A}$ as

$$\mathbf{A} = \begin{bmatrix} \frac{\partial f_1}{\partial \theta_1} & \frac{\partial f_1}{\partial \theta_2} & \cdots & \frac{\partial f_1}{\partial \theta_p} \\ \frac{\partial f_2}{\partial \theta_1} & & & \\ \vdots & & & \\ \frac{\partial f_n}{\partial \theta_1} & & \cdots & \frac{\partial f_n}{\partial \theta_p} \end{bmatrix} \quad (6)$$

where n is the number of curve points and p the number of those unknown parameters. Since n usually exceeds p, this matrix is not in general square. By differentiating Eq. (2), the elements of the gradient vector necessary for the application of steepest descent are given by

$$\frac{\partial Q}{\partial \theta_{\mathbf{k}}} = \sum_{i=1}^{p} 2 f_i \frac{\partial f_i}{\partial \theta_k} \quad (7)$$

so that the gradient vector $\mathbf{g}$:

$$\mathbf{g} = \begin{bmatrix} \frac{\partial Q}{\partial \theta_1} \\ \vdots \\ \frac{\partial Q}{\partial \theta_p} \end{bmatrix} = 2 \begin{bmatrix} \frac{\partial f_1}{\partial \theta_1} & \cdots & \frac{\partial f_n}{\partial \theta_1} \\ \vdots & & \\ \frac{\partial f_1}{\partial \theta_p} & \cdots & \frac{\partial f_n}{\partial \theta_p} \end{bmatrix} \begin{bmatrix} f_1 \\ \vdots \\ f_n \end{bmatrix} \quad (8)$$

that is

$$\mathbf{g} = 2\mathbf{A}\mathbf{f}' \quad (9)$$

where $\mathbf{f}' = [f_1, \ldots, f_n]$. Now differentiating (7) with respect to θ_j we get

$$\frac{\partial^2 Q}{\partial \theta_k \partial \theta_j} = 2 \sum_{i=1}^{n} \frac{\partial f_i}{\partial \theta_j} \frac{\partial f_i}{\partial \theta_k} + 2 \sum_{i=1}^{n} f_i \frac{\partial^2 f_i}{\partial \theta_j \partial \theta_k} \quad (10)$$

If we assume that the second term in (10) may be neglected we have

$$\frac{\partial^2 Q}{\partial \theta_k \partial \theta_j} \approx 2 \sum_{i=1}^{n} \frac{\partial f_i}{\partial \theta_j} \frac{\partial f_i}{\partial \theta_k} \quad (11)$$

These are the elements of the Hessian matrix $\mathbf{H}$, which may therefore be written in the form

$$\mathbf{H} \approx \mathbf{2A'A} \quad (12)$$

The classical Newton-Raphson minimization method is

$$\Theta_{i+1} = \Theta_i - \lambda_i \mathbf{H}^{-1}(\Theta_i)\mathbf{g}(\Theta_i) \quad (13)$$

where $\lambda_i$is determined by a linear search from Θ_i in the direction $-\mathbf{H}^{-1}\mathbf{g}$. A modification of (13) suggested first by Levenberg is to use the following:

$$\Theta_{i+1} = \Theta_i - [\lambda \mathbf{I} + \mathbf{A'A}]^{-1}(\mathbf{A'f}) \quad (14)$$

where λ is a scalar which may be adjusted to control the sequence of iterations and $\mathbf{I}$ is the $(p \times p)$ identity matrix. In general $\mathbf{A'A}$ is positive definite so the procedure should converge. We use λ to control the iterative procedure. This enables the method to take advantage of the reliable improvement given by steepest descent when still far from the minimum, and the rapid convergence of Newton-Raphson when close to the minimum.

3. MR IMAGE MORPHING

We assume the rigid registration, between the US template shape C_{TU} and the MR template shape C_{TM}, is given by the transformation T_p. After the segmentation, we get a realtime organ's shape C_r based on the prior US shape C_{TU} and the content of the realtime US image. Meanwhile, we know the rigid transformation T_r between the US prior shape and the realtime shape.

3.1. Extraction of Evolving Path

Initially, there are several feature points on these two templates. These points are labelled by experts to point out some important features of medical structures. They are one-to-one corresponding. After the segmentation process, the same feature points are labelled out on the realtime US shape. Because it is possible that some structures are missing in each image, the number of feature points on the realtime shape may not equal to that on the MR template.

We apply the radial projection technique to map these feature points to each other. Radial projection works for convex contours. The points on the contour are mapped on a circle of radius R from one point inside the contour:

$$\mathbf{q} = R\frac{\mathbf{p} - \mathbf{p_o}}{||\mathbf{p} - \mathbf{p_0}||} \tag{15}$$

where $\mathbf{p}$ is a point on the contour, $\mathbf{p_0}$ is the selected inside point and $\mathbf{q}$ is the corresponding radial projection point on the circle.

Before applying the radial projection, it is necessary to convert the original curves, contour $T_{\mathrm{r}}(C_{\mathrm{r}})$ and $T_{\mathrm{p}}(C_{\mathrm{TM}})$, into convex contour. We implement this conversion based on a simplified level set method where the speed depends only on the curvature:

$$F = -\varepsilon k; \tag{16}$$

where ε is a positive constant.

At each iteration of the evolution process, only the vertices of the concave parts of the curve must evolve. When an evolution is applied to concave vertices, they move in the normal direction. The evolution process of a curve is applied until the polygon becomes convex polygons. Finally, we get two convex polygons E_{TM} and E_r from the transformed curves $T_p(C_{TM})$ and $T_r(C_r)$, respectively.

Then we project polygons E_{TM} and E_r in circles of the same radius. Because there are some points in the convex polygons that present several points on the original curves, the projection of the collapsed points must be reconstructed in the circle. The projected vertices on the circles from each of the curves are merged, resulting in a polygon inscribed on the circle containing all points q_i from both convex curves. These points on the new polygon are then mapped back onto each of the transformed curves $T_{\mathrm{p}}(C_{\mathrm{TM}})$ and $T_{\mathrm{r}}(C_{\mathrm{r}})$.

3.2. Deformation Simulation

Once we obtain the corresponding feature points on these two transformed curves $T_p(C_{TM})$ and $T_r(C_r)$, a rigid transformation $D(\theta, T)$ is computed which gives an alignment between these two curves using the point correspondence. This is done by minimizing the sum of the distances between all pairs of corresponding feature points. We interpolate linearly the rotation from the zero to θ and also the translation with the parameter β, $\beta \in [0, 1]$. For each β, we have two transformations $D_1(\beta\theta, \beta T)$ and $D_2((1-\beta)\theta, (1-\beta)T)$. Then we get two new curves produced by applying D_1 on $T_p(C_{TM})$ and D_2 on $T_r(C_r)$. To compute the transformation of the MR template shape in the time β, we use a linear interpolation of the correspond points in the two new curves for each β. This process leads to a simulation of the deformation of the organ on the MR image space, according to the realtime ultrasound image.

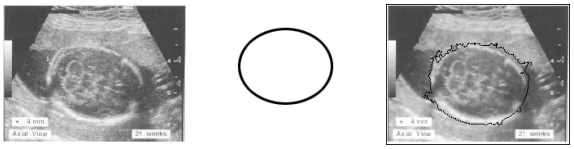

(a) (b) (c)

Fig. 1. The segmentation result of an US image with an incomplete brain. (a) The test US image, (b) The training circular shape, (c) The estimated closed brain contour.

4. EXPERIMENTAL RESULTS

We set up the operation room and conduct the calibration procedure basically following [9]. The system consists of a magnetic position tracker, a commercially available US scanner (ATL), and a 930-MHz Pentium III PC.

Fig. 1 is an example to illustrate the performance of our shape prior based segmentation method. We applied an incomplete US brain image (Fig. 1(a)) as the test image and assumed the outline of this organ was just a closed elliptical curve as shown in Fig. 1(b). The segmentation in Fig. 1(c) shows that our method can successfully deal with boundary leak using shape prior constraints.

Fig. 2 is another segmentation experiment on a MR fetus image. The shape of the fetus in Fig. 2(a) is clear and completed. Using its outline as a shape prior, Fig. 2(b) was segmented using our method and the result is shown in Fig. 2(c). We can see even there are some missing structures (arms and angles) in the test image, the obtained shape is very similar to the training shape while there are some local deformation due to the difference between the test image and the training image. The segmentation time depends on the input images and the initialization contours. In our experiments, the average segmentation time is 2.8s.

The application of the proposed method in simulation of organ's deformation is shown in Fig.3. Fig. 3(a) shows the pre-operative US image with the shape of ROI. Fig.3(b) is the reformatted MR image corresponding to the ultrasonography depicted location. The intra-operative US image and the real-time shape of the ROI are shown in Fig.3(c) and the simulated MR image is shown in Fig.3(d).

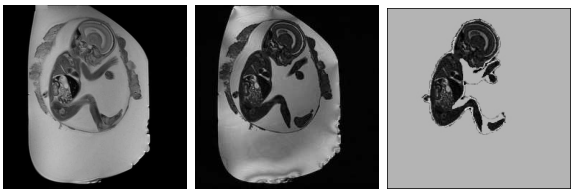

(a) (b) (c)

Fig. 2. The segmentation result of a MR image containing an incomplete fetus. (a) The training image with complete fetus outlier, (b) The test image to be segmented, (c) The final segmented closed shape of the fetus.

5. CONCLUSIONS

In this paper, a novel real-time approach is presented to correct organ deformation. We proposed a simple shape prior based segmentation method in which shape prior knowledge is incorporate into the geodesic active contours scheme by an edge matching technique. Fast matching is obtained by using the matching gradient of the contour's points. Another contribution of this paper is a procedure to simulate organ deformation using the results of the proposed segmentation process. We applied the proposed approach on several medical images. The results show that our segmentation method is robust as well as fast and the deformation correction procedure can give a good performance. Those properties can help the clinicians in anatomical structure reconstruction and image-guided surgery.

6. REFERENCES

[1] T. Cootes, C. Taylor, D. Cooper, and J. Graham, "Active shape models-their training and application," *Comput. Vis. Image Understanding*, vol. 61, pp. 38–59, 1995.

[2] T. Arbel, X. Morandi, R.M. Comeau, and D. L. Collins, "Automatic non-linear mri-ultrasound registration for the correction of intra-operative brain deformations," in *Medical Image Computing and Computer Assisted Intervention-MICCAI*, Utrecht,Netherlands, Oct. 2001, pp. 913–922.

[3] X. Pennec, N. Ayache, A. Roche, and P. Cachier, "Non-rigid mr/us registration for tracking brain deformations," in *Proc. Medical Imaging and Augmented Reality*, Shatin, HongKong, June 2001, pp. 79–86.

[4] S. Aylward, J. Jomier, J.P. Guyon, and S. Weeks, "Intraoperative 3d ultrasound augmentation," in *IEEE International Symposium on Biomedical Imaging*, Washington,USA, July 2002, pp. 421–424.

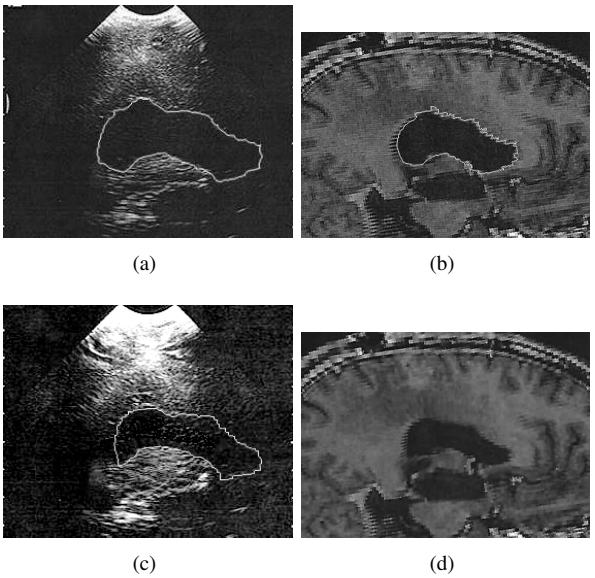

(a) (b) (c) (d)

Fig. 3. An example of real-time simulation of MR image. (a) The preoperative US image with the shape of ROI, (b) The reformatted MR image corresponding to the ultrasonography depicted location, (c) The intra-operative US image and the real-time shape of the ROI, (d) The simulated MR image.

[5] M. Rousson and N. Paragios, "Shape prior for level set representation," in *Proc. Int. Conf. Image Processing*, Kobe, Japan, Oct. 1999, pp. 188–192.

[6] M. Leventon, E. Grimson, and O. Faugeras, "Statistical shape influence in geodesic active contours," in *Proc. IEEE Conf. Computer Vision and Pattern Recognition*, South Carolina, USA, June 2000, pp. 316–322.

[7] A. Tsai, A. Yezzi, W. Wells, and A. Willsky, "Model-based curve evolution technique for image segmentation," in *Proc. IEEE Conf. Computer Vision and Pattern Recognition*, Hawaii, USA, Dec. 2001, vol. I, pp. 463–468.

[8] Y. Chen, H. Thiruvenkadam, and D. Wilson, "On the incorporation of shape priors into geometric active contours," in *Proc. IEEE International Workshop on Variational and Level Set Methods*, Vancouver, Canada, July 2001, pp. 145–152.

[9] N. Pagoulatos, W.S. Edwards, D.R. Haynor, and Y. Kim, "Interactive 3d registration of ultrasound and magnetic resonance images based on a magnetic position sensor," *IEEE Transactions on Information Technology in Biomedicine*, vol. 3, no. 4, pp. 278–288, 1999.